Optics Letters

Y4-Net: a deep learning solution to one-shot dual-wavelength digital holographic reconstruction

KAIQIANG WANG,[1] QIAN KEMAO,[2,3] JIANGLEI DI,[1,4] AND JIANLIN ZHAO[1,*]

[1]MOE Key Laboratory of Material Physics and Chemistry under Extraordinary Conditions, Shaanxi Key Laboratory of Optical Information Technology, School of Physical Science and Technology, Northwestern Polytechnical University, Xi'an 710129, China
[2]School of Computer Science and Engineering, Nanyang Technological University, Singapore 639798, Singapore
[3]e-mail: mkmqian@ntu.edu.sg
[4]e-mail: jiangleidi@nwpu.edu.cn
*Corresponding author: jlzhao@nwpu.edu.cn

Received 17 April 2020; revised 12 June 2020; accepted 29 June 2020; posted 30 June 2020 (Doc. ID 395445); published 27 July 2020

In this Letter, a deep learning solution (Y4-Net, four output channels network) to one-shot dual-wavelength digital holography is proposed to simultaneously reconstruct the complex amplitude information of both wavelengths from a single digital hologram with high efficiency. In the meantime, by using single-wavelength results as network ground truth to train the Y4-Net, the challenging spectral overlapping problem in common-path situations is solved with high accuracy.

https://doi.org/10.1364/OL.395445

Digital holography (DH), as a dynamic, non-destructive, high-sensitivity, and full-field method for quantitative amplitude and phase measurement [1,2], has been widely used in various fields such as microscopic imaging, three-dimensional (3D) recognition, and particle and flow-field measurements [3–6].

In DH, there are two typical phase extraction methods. The first is the phase-shifting method in an in-line setup, which requires multiple holograms with different phase shifts [7]. The second is the spectral filtering method in an off-axis setup, which decreases the maximum spatial frequency of the hologram as the off-axis angle increases [8]. In both methods, the phase distribution of a wavefront calculated from the holograms is wrapped in the range of $(-\pi, \pi)$ [9]. Consequently, phase unwrapping is used to obtain the actual smooth phase distributions [10–12], which often fails when the actual phase is discontinuous. An ideal solution to the discontinuous phase is the dual-wavelength (λ_1 and λ_2) DH [13]. It provides a longer synthetic wavelength $\Lambda_1 = \lambda_1\lambda_2/|\lambda_2 - \lambda_1|$ and expands the measurement range [13]. As another application for a smooth sample, a shorter synthetic wavelength $\Lambda_2 = \lambda_1\lambda_2/|\lambda_2 + \lambda_1|$ enables increases to the measurement accuracy of phase measurement, in which the superposition effect of the two holograms with different wavelengths will reduce the speckle noise [14].

However, for dual-wavelength DH, both phase-shifting and spectral filtering solutions have their own drawbacks. The phase-shifting solution for in-line setups requires even more holograms [15]. As for the spectral filtering method, complicated off-axis optical paths based on Mach–Zehnder or Michelson interferometers are designed to generate two sets of orthogonal interference fringes in a single hologram and then adjusted to make these two sets of fringes separable in the frequency domain [16–19]. In such off-axis setups, as the object and reference beams travel along different paths, the measured phase is sensitive to the environment disturbance such as air fluctuations and mechanical vibrations.

In order to overcome this problem, lateral shearing was recently adopted to present a one-shot dual-wavelength common-path DH, which is extremely simple, compact, and insensitive to the environment [20,21]. However, because the spatial spectra of two sets of fringe patterns from different wavelengths are squeezed in one spectral domain, the spectral separation is difficult to satisfy, resulting in information loss and accuracy decrease. This is a common problem in self-interference-based common-path DH [22–28].

To visualize and explain the challenge in the spectrum separation, we capture a hologram of pollen by the dual-wavelength shearing DH system in Ref. [20] and reconstruct the phases as shown in Fig. 1(a). The captured hologram (first row) is Fourier transformed to obtain its spectrum (second row), where two side-lobes corresponding to the first-order spectra of two wavelengths are seen and further enlarged (third row). The two side-lobes are selected in both non-overlapping and overlapping manners (fourth row) and inversely Fourier transformed to obtain the corresponding phase images (fifth row for $\lambda_1 = 532$ nm and sixth row for $\lambda_2 = 632.8$ nm). For comparison, the same experiment is repeated with a single wavelength and analyzed similarly, as shown in Fig. 1(b). Although different circle sizes and locations are attempted in Fig. 1(a), information loss is observed, which is against the purpose of precision measurement. In the optical setup we used, the reference and object beams of the two wavelengths are coaxial, so the off-axis angles of the two wavelengths are always equal. Therefore, the first-order spectra of two wavelengths will always be in the same direction. The first-order spectra of the two wavelengths can be

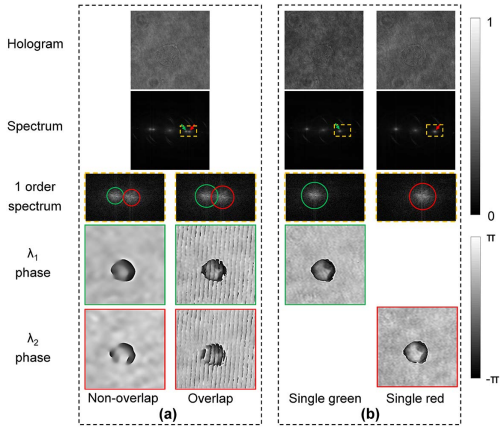

Fig. 1. Reconstruction results of different frequency regions. (a) Dual-wavelength hologram and its spatial spectrum; (b) different frequency selection regions and corresponding reconstruction results.

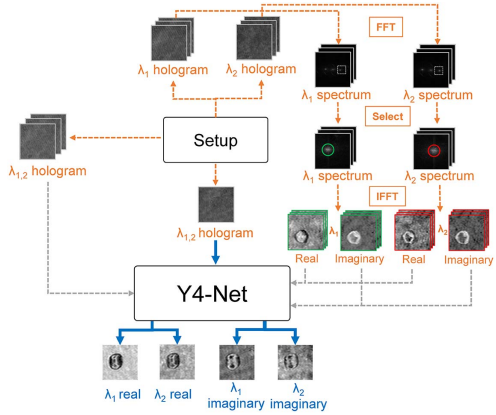

Fig. 2. Process of dataset generation (orange), network training (gray), and network testing (blue).

separated a little in the same direction by increasing the angle between the object and reference beams. But, it is limited. For the case where the two wavelengths are closer, this method is even weaker for the separation of the first-order spectra of the two wavelengths. As complete separation of the two side-lobes is difficult in a common-path setup [22–28], an intelligent hologram analysis method is sought to achieve the desired accuracy, which is the main pursuit of this Letter.

Recently, we proposed a one-to-two convolutional neural network, named Y-Net, to learn and perform the DH reconstruction [29]. Benefitting from the design of two up-sampling paths, the intensity and phase information of a wavefront can be simultaneously reconstructed [29]. However, the Y-Net is designed for the traditional single-wavelength DH. For dual-wavelength DH, to compute the synthetic wavelength, the complex amplitudes of two wavelengths should be reconstructed. In response, we improve the Y-Net by increasing the output channel number in each up-sampling path from one to two to simultaneously reconstruct the complex amplitude of the two wavelengths. The complex amplitude of the wavefront of wavelength λ_i can be equivalently represented either by the exponential form $e_i = a_i * \exp(j\varphi_i)$ or by the Cartesian form $e_i = R_i + j * I_i$ $(i = 1, 2)$. In this work, we adopt the Cartesian form. R_1 and R_2 are reconstructed in one up-sampling path due to the similarity of them. I_1 and I_2 are reconstructed in the other up-sampling path due to the same reason. Since the improved network has four output channels, we name it Y4-Net. As we are going to show, Y4-Net has high efficiency through the simultaneous reconstruction of two wavefronts for dual-wavelength DH and also high accuracy by learning to separate the side-lobes for common-path situations.

As has been emphasized earlier, the key problem for common-path situations is to solve the spectrum separation problem so that better accuracy can be achieved even with the overlapping side-lobes. Therefore, the Y4-Net is trained with guidance from the high-quality complex amplitude without overlap as the ground truth. To get the ground truth, we add two shutters for each wavelength in the experimental setup in Ref. [20] and capture the holograms with only one wavelength at each time, whose reconstruction results are denoted as R_i^T and I_i^T $(i = 1, 2)$ and also shown in Fig. 1(b) corresponding to the example in Fig. 1(a). We can see that the spectra of the single-wavelength holograms can be chosen to be a larger size to retain sufficient spectral information. Consequently, we use dual-wavelength holograms as network input and use the single-wavelength results as the ground truth to train the Y4-Net. This idea is illustrated in Fig. 2, which has three parts including dataset generation (orange dotted lines), network training (gray dotted lines), and network testing (blue solid lines).

In the dataset generation, the used samples are pollens. A total of 500 dual-wavelength holograms are recorded. Correspondingly, the single-wavelength holograms are recorded and then used to get the real and imaginary parts of the complex amplitudes of the two wavelengths by the spectral filtering method. When recording the holograms, the CCD target is located on the image plane of the samples. The dual-wavelength holograms are used as inputs. The real and imaginary parts of the complex amplitudes of the two wavelengths are used as ground truth. All the data are partitioned into 80% for training, 10% for validating (overfitting detection), and 10% for testing.

In network training, the mean squared errors (MSE) of real and imaginary parts from their respective up-sampling paths are separately calculated as

$$L_R = \frac{1}{N}\sum_{n}^{N}[(R_{1,n}^T - R_{1,n})^2 + (R_{2,n}^T - R_{2,n})^2], \quad (1)$$

$$L_I = \frac{1}{N}\sum_{n}^{N}[(I_{1,n}^T - I_{1,n})^2 + (I_{2,n}^T - I_{2,n})^2], \quad (2)$$

where $R_{i,n}^T$ and $I_{i,n}^T$ are the ground truth of the real and imaginary parts, $R_{i,n}$ and $I_{i,n}$ are the network-reconstructed real and imaginary parts; i can take 1 and 2 to represent λ_1 and λ_2, respectively, n is the number of the training dataset, and N is the mini-batch size. To associate real and imaginary parts, the following sum of the loss functions is back-propagated through the network:

$$L = L_R + L_I. \quad (3)$$

The Adam optimizer [30] with a learning rate of 0.002 (halved after every 15 epochs) and the mini-batch size of 32 are adopted to update the network's parameters. The Y4-Net has 16M parameters and is implemented using Pytorch. All of the experiments are performed on a PC with Core i7-8700K CPU

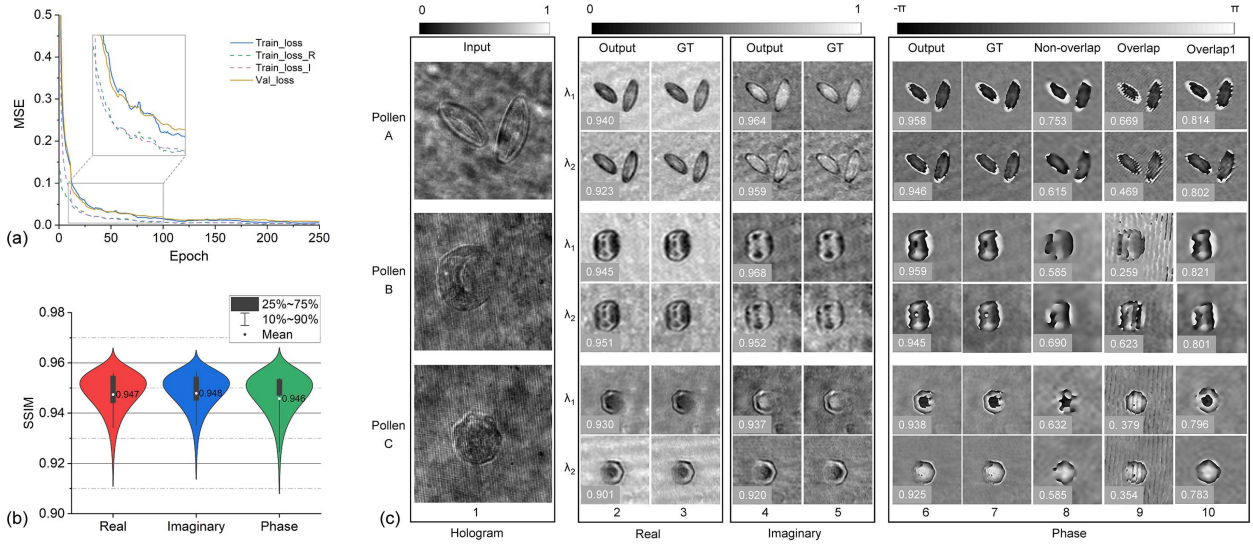

Fig. 3. Y4-Net training and testing. (a) Plot of loss functions in Y4-Net training; (b) violin plot of the SSIM for the testing dataset; (c) testing results of three typical examples and their comparisons with traditional methods. In (c), the column number is below each column, and the SSIM value is inserted in the lower-left corner of each result image.

(3.8 GHz) and 16 GB of RAM, using NVIDIA GeForce GTX 1080Ti GPU. As shown in Fig. 3(a), the training and validating loss functions gradually converge as the learning progress, in which we can see that overfitting does not appear. To investigate how L_R and L_I contribute to L in the learning process, we also plot L_R and L_I by dotted lines, as the learning progress in Fig. 3(a). It can be seen from the enlarged part that during the learning process, L_R and L_I alternately fall, which have almost the same contribution to L.

In network testing, the Y4-Net is randomly given a dual-wavelength hologram from the testing dataset and simultaneously outputs both real and imaginary parts of the complex amplitudes of two wavelengths. Then, the wrapped phase is calculated from the complex amplitude. As shown in Fig. 3(b), we count the structural similarity index (SSIM) value of each test result in a violin plot [31]. It can be seen that the trained Y4-Net performs well in the entire testing dataset. More visually, the reconstruction results of three different pollens randomly picked from the testing dataset are shown in Fig. 3(c). From a dual-wavelength hologram (first column), the trained Y4-Net reconstructs the complex amplitude information of the two wavelengths with the form of real and imaginary parts (second and fourth columns). More intuitively, we calculate the corresponding phase from the complex amplitude of the network output and ground truth (sixth and seventh columns). For comparison, we also show the traditional reconstruction results of spectral non-overlap and overlap (eighth and ninth columns). Further, we use a mask to shield the corresponding overlapping part of the overlap results and obtain the results overlap1 (tenth column). The SSIM is inserted in the lower-left corner of each result image. The SSIM indices between the network results and ground truth are higher than the traditional manual spectrum separation method. For phase reconstruction quality, the mean SSIM of the testing dataset increases from 0.652 (non-overlap), 0.511 (overlap), and 0.805 (overlap1) to 0.946 (Y4-Net).

To further verify the effect of Y4-Net in synthesizing longer and shorter wavelengths (Λ_1 and Λ_2 mentioned in the second paragraph), we use a high-power laser to ablate the surface of the quartz glass to generate many small pits and use them as samples to make a dataset following the steps described in the orange part of Fig. 2. Then, we use the pit dataset to train and test the Y4-Net and reconstruct the results of an example as the synthetic wavelength Λ_1 form, as shown in the upper part of Fig. 4. Similarly, the pollen-trained Y4-Net is previously used to get the corresponding results of an example as the synthetic wavelength Λ_2 form, as shown in the lower part of Fig. 4. First, we input the holograms (first column) into the trained Y4-Net and get the complex amplitude of λ_1 and λ_2 (second and third columns). Second, the wrapped phases (fourth column) of λ_1 and λ_2 are calculated from the complex amplitude. Lastly, we get the wrapped phase of the synthetic wavelength from the complex amplitude of λ_1 and λ_2 and unwrapped it by MATLAB's unwrap function (fifth and sixth columns). For the pit, the wrapped phases of λ_1 and λ_2 have four and five wraps, respectively. But, when converted to a synthetic wavelength Λ_1 form, the phase contains only one wrap, which will avoid discontinuity in the wrapped phase for steep samples [13]. For the pollen, the wrapped phases of λ_1 and λ_2 have one wrap. But, when converted to a synthetic wavelength Λ_2 form, the phase contains three wraps, which increases the measurement accuracy and reduces the speckle noise for the smooth sample [14].

In all the experiments, we use fixed optical setup parameters (such as off-axis angle, wavelength, de-focus distance, and magnification) to obtain the dataset. Therefore, the trained network can only be effective in a small range around the original optical setup parameters. In practical applications, we recommend to randomly change the optical setup parameters within a certain range when collecting the dataset, so that the trained neural network has a better tolerance for different optical setup parameters. The pollens and pits in our experiments contain only a small amount of detailed information. When using more complex samples as the dataset, the network performance may be slightly reduced.

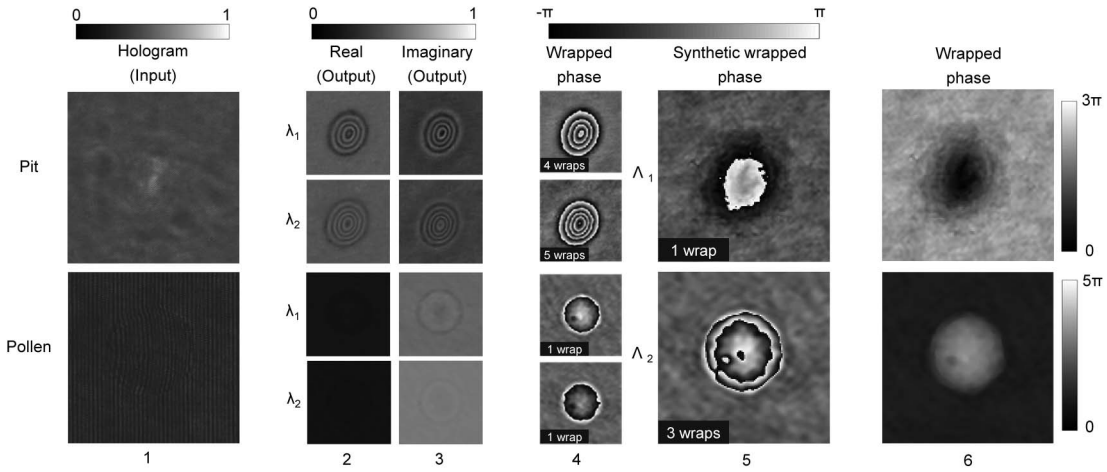

Fig. 4. Reconstruction results of the example pit and pollen for single and synthetic wavelengths. The column number is below each column. The wrap count is inserted in the lower-left corner of each wrapped phase.

To summarize, in this Letter, hinted by the Y-Net [29], we have proposed and demonstrated the specially designed Y4-Net for simultaneous reconstruction of the complex amplitude information of two wavelengths from a single dual-wavelength digital hologram. The Y4-Net not only improves the reconstruction efficiency, but also successfully solves the problem of spectral overlap and improves the phase reconstruction accuracy of one-shot dual-wavelength common-path DH. Notably, the Y4-Net is also applicable to non-common-path situations without the problem of spectral overlap.

Funding. National Natural Science Foundation of China (61927810); The Joint Fund of the National Natural Science Foundation of China and the China Academy of Engineering Physics NSAF (U1730137); The Fundamental Research Funds for the Central Universities (3102019ghxm018).

Disclosures. The authors declare no conflicts of interest.

REFERENCES

1. D. Gabor, Nature **161**, 777 (1948).
2. J. W. Goodman and R. W. Lawrence, Appl. Phys. Lett. **11**, 77 (1967).
3. W. S. Haddad, D. Cullen, J. C. Solem, J. W. Longworth, A. Mcpherson, K. Boyer, and C. K. Rhodes, Appl. Opt. **31**, 4973 (1992).
4. B. Javidi and E. Tajahuerce, Opt. Lett. **25**, 610 (2000).
5. G. Pan and H. Meng, Appl. Opt. **42**, 827 (2003).
6. T. Xi, J. Di, Y. Li, S. Dai, C. Ma, and J. Zhao, Opt. Express **26**, 28497 (2018).
7. I. Yamaguchi and T. Zhang, Opt. Lett. **22**, 1268 (1997).
8. E. Cuche, P. Marquet, and C. Depeursinge, Appl. Opt. **39**, 4070 (2000).
9. M. D. Pritt and D. C. Ghiglia, *Two-Dimensional Phase Unwrapping: Theory, Algorithms, and Software* (Wiley, 1998).
10. M. D. Pritt and J. S. Shipman, IEEE Trans. Geosci. Remote Sens. **32**, 706 (1994).
11. M. Zhao, L. Huang, Q. Zhang, X. Su, A. Asundi, and Q. Kemao, Appl. Opt. **50**, 6214 (2011).
12. J. M. Huntley and H. Saldner, Appl. Opt. **32**, 3047 (1993).
13. C. Wagner, W. Osten, and S. Seebacher, Opt. Eng. **39**, 79 (2000).
14. J. Di, Y. Song, T. Xi, J. Zhang, Y. Li, C. Ma, K. Wang, and J. Zhao, Opt. Eng. **56**, 111712 (2017).
15. T. Tahara, R. Mori, S. Kikunaga, Y. Arai, and Y. Takaki, Opt. Lett. **40**, 2810 (2015).
16. J. Kühn, T. Colomb, F. Montfort, F. Charrière, Y. Emery, E. Cuche, P. Marquet, and C. Depeursinge, Opt. Express **15**, 7231 (2007).
17. A. Khmaladze, M. Kim, and C. Lo, Opt. Express **16**, 10900 (2008).
18. D. G. Abdelsalam, R. Magnusson, and D. Kim, Appl. Opt. **50**, 3360 (2011).
19. J. Min, B. Yao, P. Gao, R. Guo, B. Ma, J. Zheng, M. Lei, S. Yan, D. Dan, T. Duan, Y. Yang, and T. Ye, Appl. Opt. **51**, 191 (2012).
20. J. Di, Y. Li, M. Xie, J. Zhang, C. Ma, T. Xi, E. Li, and J. Zhao, Appl. Opt. **55**, 7287 (2016).
21. J. Di, Y. Song, T. Xi, J. Zhang, Y. Li, C. Ma, K. Wang, and J. Zhao, Opt. Eng. **56**, 111712 (2017).
22. Q. Weijuan, Y. Yingjie, C. O. Choo, and A. Asundi, Opt. Lett. **34**, 1276 (2009).
23. W. Qu, K. Bhattacharya, C. O. Choo, Y. Yu, and A. Asundi, Appl. Opt. **48**, 2778 (2009).
24. V. Chhaniwal, A. S. Singh, R. A. Leitgeb, B. Javidi, and A. Anand, Opt. Lett. **37**, 5127 (2012).
25. A. S. Singh, A. Anand, R. A. Leitgeb, and B. Javidi, Opt. Express **20**, 23617 (2012).
26. K. Lee and Y. Park, Opt. Lett. **39**, 3630 (2014).
27. K. Kim, Z. Yaqoob, K. Lee, J. W. Kang, Y. Choi, P. Hosseini, P. T. C. So, and Y. Park, Opt. Lett. **39**, 6935 (2014).
28. D. Roitshtain, N. A. Turko, B. Javidi, and N. T. Shaked, Opt. Lett. **41**, 2354 (2016).
29. K. Wang, J. Dou, Q. Kemao, J. Di, and J. Zhao, Opt. Lett. **44**, 4765 (2019).
30. D. P. Kingma and J. Ba, "Adam: A method for stochastic optimization," arXiv preprint arXiv: 1412.6980 (2014).
31. Z. Wang, A. C. Bovik, H. R. Sheikh, and E. P. Simoncelli, IEEE Trans. Image Process **13**, 600 (2004).